Two unusual nanosized Nd^{3+}-substituted selenotungstate aggregates simultaneously comprising lacunary Keggin and Dawson polyoxotungstate segments

Hailou Li,[a,b] Chen Lian,[b] Lijuan Chen, [a,*] Junwei Zhao,[a,*] and Guo-Yu Yang [b,*]

[a]Henan Key Laboratory of Polyoxometalate Chemistry, College of Chemistry and Chemical Engineering, Henan University, Kaifeng, Henan 475004, China

[b]MOE Key Laboratory of Cluster Science, School of Chemistry and Chemical Engineering, Beijing Institute of Technology, Beijing 102488, China

Supporting Information

Fig. S1 Experimental and simulated PXRD patterns of **1** and **2**.

Fig. S2 (a) The POA of $[(W_3Eu_2(H_2O)_8AsO_8(OH))(B\text{-}\alpha\text{-}AsW_9O_{33})_2]_2^{16-}$**.** (b) The POA of $\{[W_3Nd_2(H_2O)_3(NO_3)O_6](B\text{-}\alpha\text{-}SeW_9O_{33})_2(\alpha\text{-}Se_2W_{14}O_{52})\}^{17-}$. (c) The $\{Eu_2W_3\}$ cluster. (d) The $\{Nd_2W_3\}$ cluster.

Fig. S3 (a) The POA of **1**. (b) The trimer of $\{Se_6W_{35}\}$.

Fig. S4 (a) Simplified view of the stacking of **1a** POAs along the *b* axis. (b) Simplified view of the stacking of **1a** POAs along the *c* axis.

Fig. S5 (a) The POA of $\{(Pd_5Se_2)(W_3)(B\text{-}\alpha\text{-}SeW_9)(\beta\text{-}Se_2W_{14})\}_2$**.** (b) The POA of $\{[W_2Nd_2(H_2O)_8O_6(OH)_2(\beta\text{-}Se_2W_{14}O_{52})][W_3Nd_2(H_2O)_6O_7(SeW_9O_{33})_2]_2\}^{20-}$. (c) and (d) The lacunary Keggin-type $[B\text{-}\alpha\text{-}SeW_9O_{33}]^{8-}$ and Dawson-type $[\beta\text{-}Se_2W_{14}O_{52}]^{12-}$segments.

Fig. S6 (a) Simplified view of the stacking of **2a** POAs along the *b* axis**.** (b) Simplified view of the stacking of **2a** POAs along the *c* axis.

Fig. S7 (a-b) TGA curves of **1** and **2**.

Fig. S8 (a-b) IR spectra of **1** and **2**.

Fig. S9 Comparison of IR spectra of the fresh **2** (fresh), the catalyst after the first cycle (1), the catalyst after the second cycle (2), the catalyst after the third cycle (3), the catalyst after the fourth cycle (4) and the catalyst after the fifth cycle (5).

Fig. S10 The possible mechanism for oxidation of thioethers catalyzed by **2**.

Table S1. The results of BVS calculations of all O atoms in **1a**.

Table S2. The results of BVS calculations of all O atoms in **2a**.

Table S3. Comparison of some POM-based catalysts for the catalytic oxidation of MPS with **2**.

Materials and methods

All chemicals were commercially purchased and used without further purification. C, H and N elements were measured on a Vario EL Cube CHNS analyzer. The contents of Na, K, W, Nd, and Se elements were measured by inductively coupled plasma atomic emission spectrometry (ICP–AES) on a Perkin–Elmer Optima 2000 ICP–AES spectrometer. IR spectra were recorded from solid sample palletized with KBr on a Perkin−Elmer FT−IR spectrometer in the range 400−4000 cm^{-1}. Powder X-ray diffraction (PXRD) patterns were collected on a Bruker D8 ADVANCE instrument with Cu Kα radiation (λ = 1.54056 Å). TG analyses were performed under a N_2 atmosphere on a Mettler–Toledo TGA/SDTA 851^e instrument with a heating rate of 20 °C min^{-1} from 30 to 1000 °C. The GC chromatograms were obtained on a SHIMADZU GC-2014C.

X-ray crystallography

The suitable crystals of **1** and **2** were picked and sealed to a glass tube closed at both ends. Intensity data for **1** and **2** were collected on a Bruker APEX II CCD detector at 296(2) K with Mo Kα monochromated radiation (*λ* = 0.71073 Å). Direct methods were used to solve their structures and locate the heavy atoms using the SHELXTL–97 program package.[1-2] The remaining atoms were found from successive full-matrix least-squares refinements on F^2 and Fourier syntheses. Lorentz polarization and SADABS corrections were applied. All hydrogen atoms attached to carbon and nitrogen atoms were geometrically placed and refined isotropically as a riding model using the default SHELXTL parameters. There are still solvent accessible voids in the check cif report of crystal structure, which suggest that some solvent water molecules should exist in the structure of **2** that can't be found from the weak residual electron peaks. These solvent molecules are highly disordered, and attempts to locate and refine them were unsuccessful. On the basis of elemental analysis and TG analysis, 56 lattice water molecules were directly added to the molecular formula. The crystallographic data and structure refinement parameters for **1** and **2** are listed in Table 1.

Thermogravimetric (TG) analysis

To determine the number of lattice water molecules of **1** and **2**, the TG analyses of **1** and **2** have been investigated under the flowing N_2 atmosphere with a heating rate of 10 °C min^{-1} from 30 to 1000 °C. As shown in Fig. S7a, **1** exhibits a two-step weight loss process. From 30 to 250 °C, the first weight loss of 6.05 % (calcd. 6.12%) for **1** corresponds to the release of 35 lattice water molecules. Subsequently, an apparent weight loss ranging from 250 to 700 is 5.34 % (calcd. 5.29%) for **1**, which is attributable to the loss of 3 coordination water molecules, 1 NO_2 and 4 SeO_2. Differently, **2** presents a three-step weight loss process (Fig. S7b). From 25 to 250 °C, the first weight loss of 8.67% (calcd. 8.59%) is due to the release of 84 lattice water molecules. The second weight loss between 250 and 570 °C is 4.77% (calcd. 4.76%), which is assigned to the liberration of 20 coordination water molecules, the dehydration of 16 protons and 2 hydroxyl groups, and the removal of 7 dimethylamine groups. The third weight between 570 and 700 °C is 3.98% (calcd. 3.78%), which is ascribed to the loss of 6 SeO_2. Apparently, the experimental values coincide with the theoretical values.

FT-IR spectra

IR spectra of **1** and **2** have been recorded between 4000–400 cm^{-1} by utilizing KBr pellets (Fig. S8). In the low-wavenumber region, IR spectra of **1** and **2** show the characteristic vibration patterns derived from the ST skeletons, four absorption bands attributable to ν(W–O_t), ν(Se–O), ν(W–O_b) and ν(W–O_c) are observed at 962, 885, 845 and 773 cm^{-1} for **1**, and 965, 888, 862 and 781 cm^{-1} for **2**, respectively. In the high-wavenumber region, the stretching and bending absorption vibrations of O–H groups are respectively centered at 3414 cm^{-1} and 1628 cm^{-1} for **1**,

3425 cm^{-1} and 1632 cm^{-1} for **2.** The IR spectrum of **2** has three weak bands at 3147, 2792, and 1464 cm^{-1}, which are attributed to the N–H, C–H and C–N stretching vibrations respectively, meaning the presence of dimethylamine components.

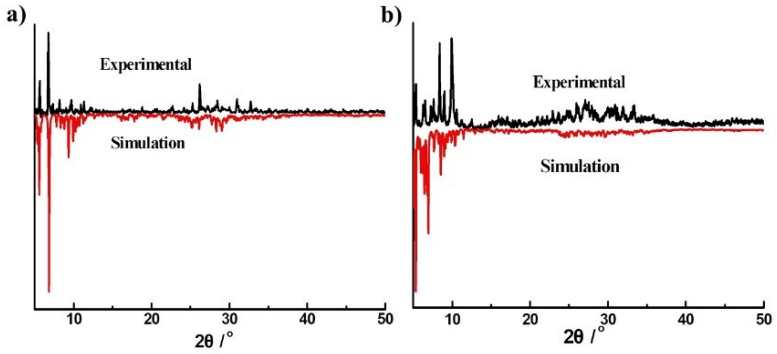

Fig. S1 Experimental and simulated PXRD patterns of **1** and **2**.

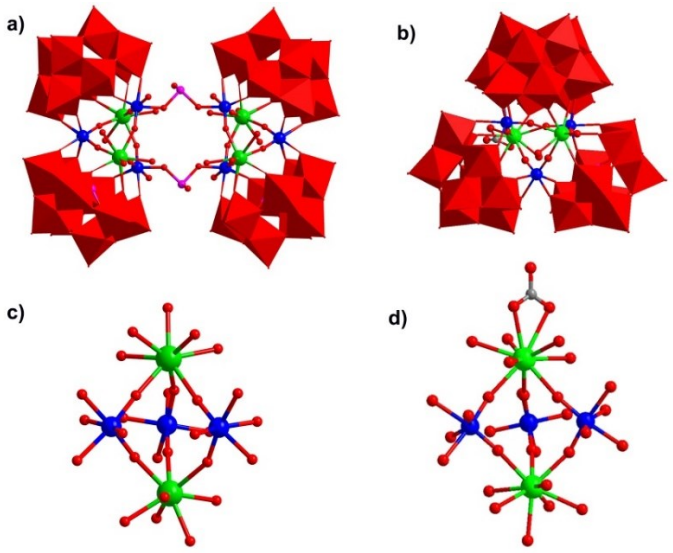

Fig. S2 (a) The POA of $[(W_3Eu_2(H_2O)_8AsO_8(OH))(B\text{-}\alpha\text{-}AsW_9O_{33})_2]_2^{16-}$**.** (b) The POA of $\{[W_3Nd_2(H_2O)_3(NO_3)O_6](B\text{-}\alpha\text{-}SeW_9O_{33})_2(\alpha\text{-}Se_2W_{14}O_{52})\}^{17-}$. (c) The $\{Eu_2W_3\}$ cluster. (d) The $\{Nd_2W_3\}$ cluster.

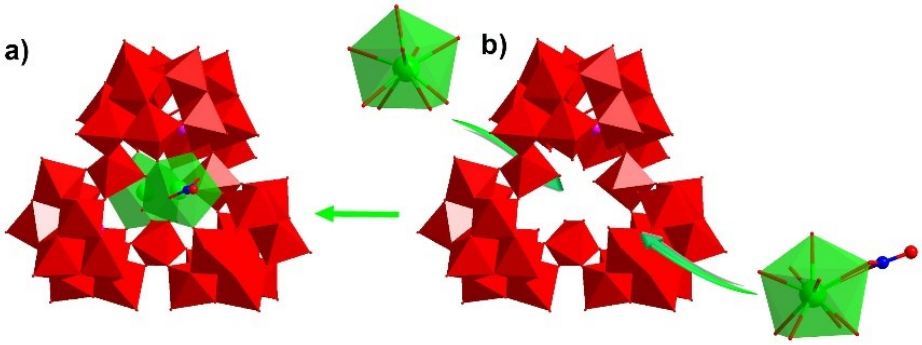

Fig. S3 (a) The POA of **1.** (b) The trimer of $\{Se_6W_{35}\}$.

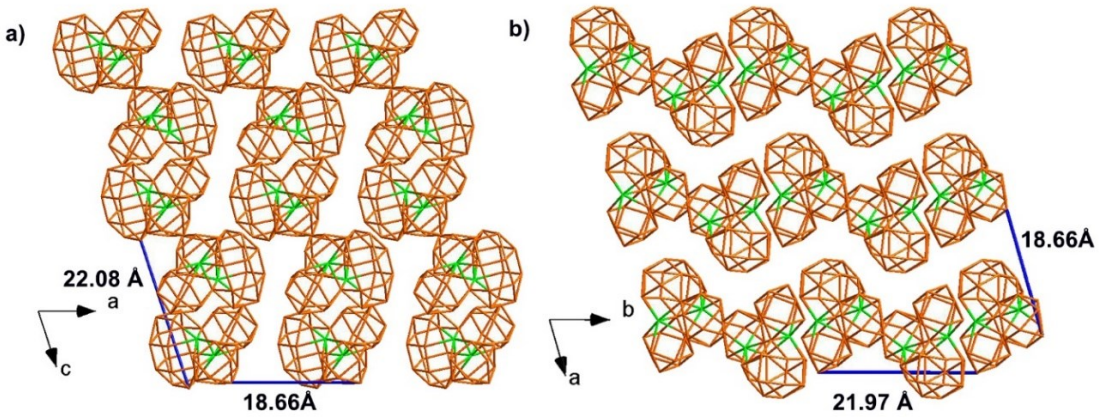

Fig. S4 (a) Simplified view of the stacking of **1a** POAs along the *b* axis. (b) Simplified view of the stacking of **1a** POAs along the *c* axis.

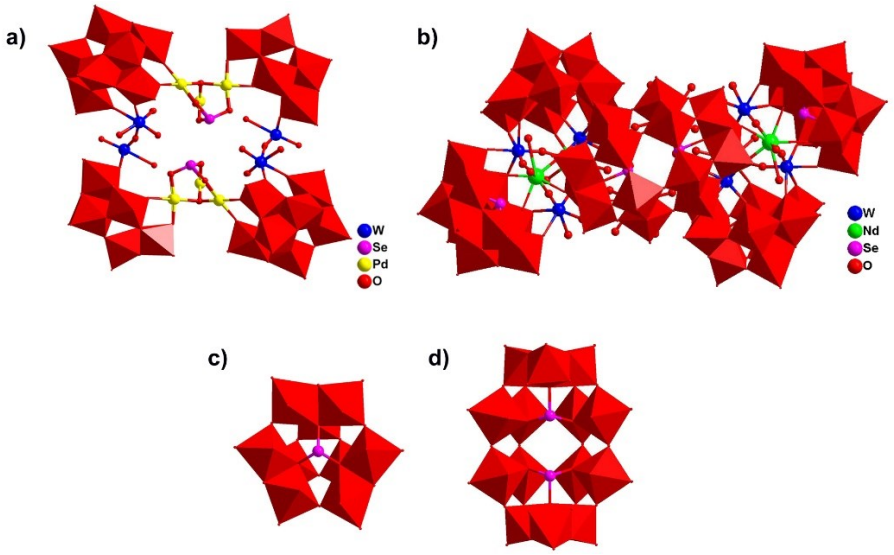

Fig. S5 (a) The POA of $\{(Pd_5Se_2)(W_3)(B\text{-}\alpha\text{-}SeW_9)(\beta\text{-}Se_2W_{14})\}_2$. (b) The POA of $\{[W_2Nd_2(H_2O)_8O_6(OH)_2(\beta\text{-}Se_2W_{14}O_{52})][W_3Nd_2(H_2O)_6O_7(SeW_9O_{33})_2]_2\}^{20-}$. (c) and (d) The lacunary Keggin-type $[B\text{-}\alpha\text{-}SeW_9O_{33}]^{8-}$ and Dawson-type $[\beta\text{-}Se_2W_{14}O_{52}]^{12-}$segments.

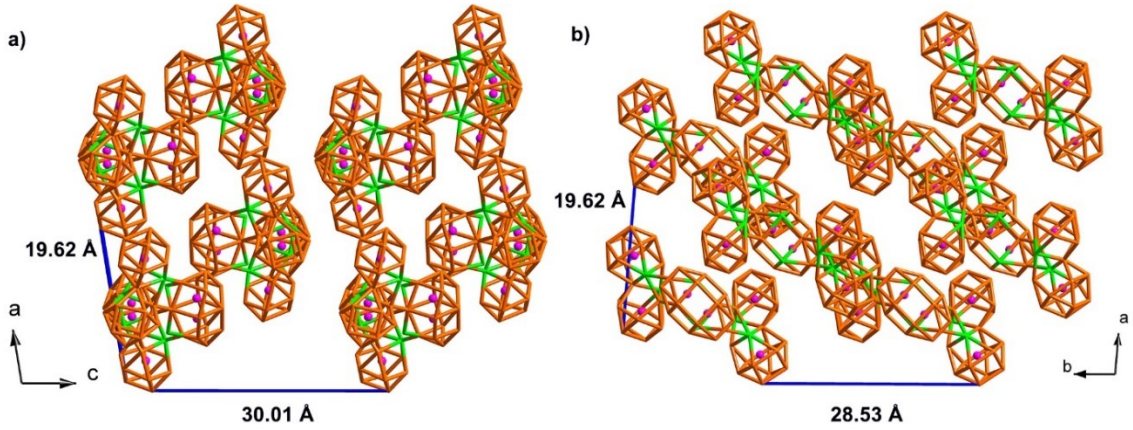

Fig. S6 (a) Simplified view of the stacking of **2a** POAs along the *b* axis**.** (b) Simplified view of the stacking of **2a** POAs along the *c* axis.

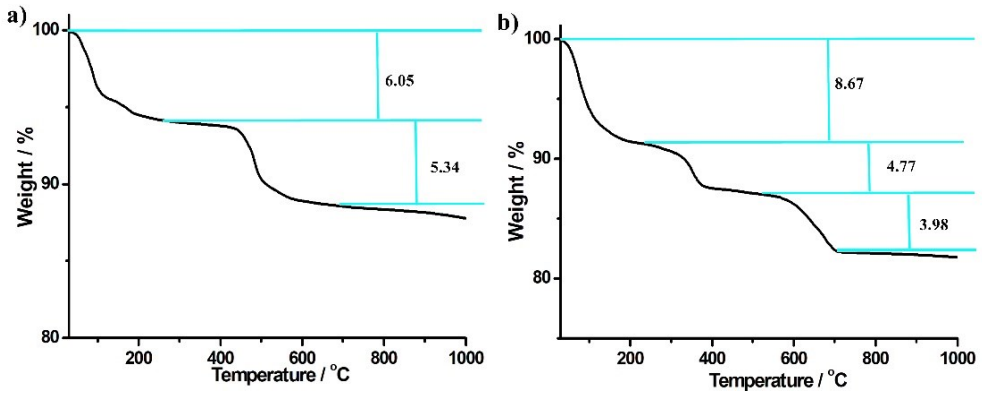

Fig. S7. (a-b) TGA curves of **1** and **2**.

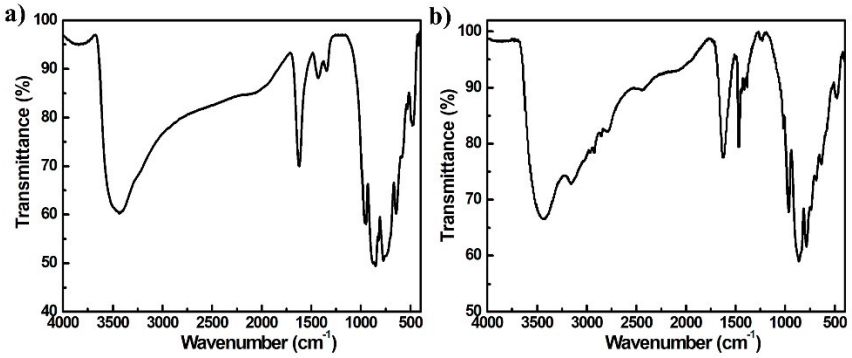

Fig. S8 (a-b) IR spectra of **1** and **2.**

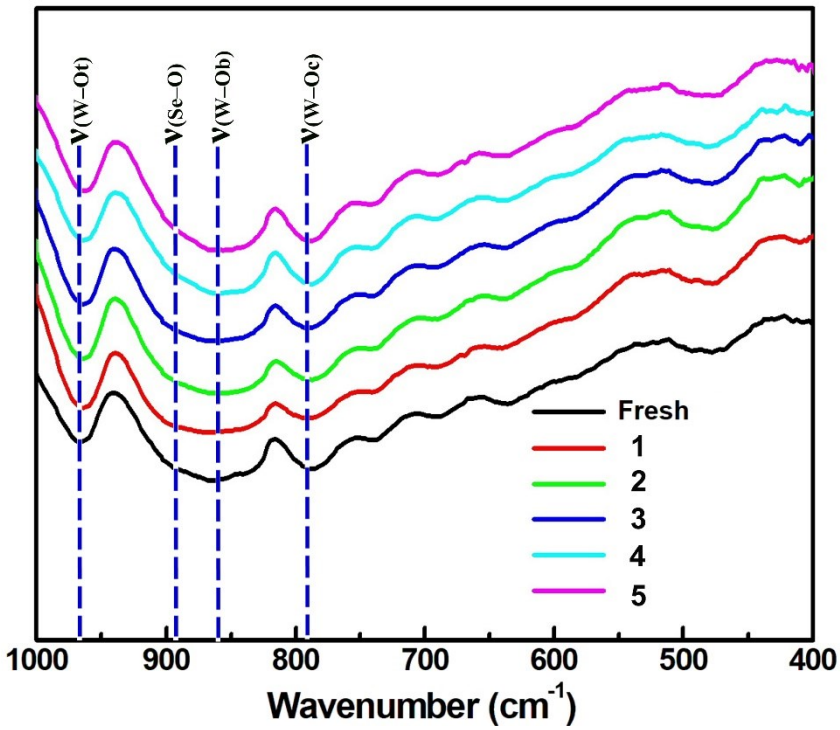

Fig. S9 Comparison of IR spectra of the fresh **2** (fresh), the catalyst after the first cycle (1), the catalyst after the second cycle (2), the catalyst after the third cycle (3), the catalyst after the fourth cycle (4) and the catalyst after the fifth cycle (5).

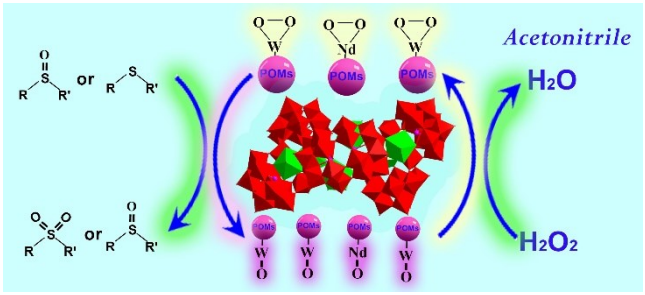

Fig. S10 The possible mechanism for oxidation of thioethers catalyzed by **2**.

Table S1. The results of BVS calculations of all O atoms in **1a**.

Atom	BVS	Atom	BVS	Atom	BVS
O1	1.920	O2	1.750	O3	1.749
O4	2.170	O5	1.859	O6	1.875
O7	1.957	O8	1.703	O9	2.004
O10	2.268	O11	1.928	O12	1.934
O13	1.979	O14	2.003	O15	1.736
O16	1.991	O17	1.908	O18	1.957
O19	1.827	O20	2.057	O21	1.876
O22	1.808	O23	1.984	O24	2.027
O25	2.160	O26	1.982	O27	1.979
O28	1.848	O29	1.798	O30	1.802
O31	2.185	O32	1.726	O33	1.849
O34	1.872	O35	1.703	O36	1.703
O37	2.061	O38	1.952	O39	2.008
O40	2.044	O41	2.079	O42	2.009
O43	1.990	O44	1.867	O45	1.995
O46	2.114	O47	1.819	O48	2.045
O49	2.036	O50	2.079	O51	2.050
O52	2.063	O53	1.875	O54	2.152
O55	2.044	O56	1.915	O57	1.809
O58	1.963	O59	1.797	O60	2.053
O61	2.003	O62	1.882	O63	1.700
O64	1.947	O65	2.008	O66	1.735
O67	1.932	O68	2.114	O69	1.859
O70	2.196	O71	1.609	O72	2.089
O73	2.032	O74	1.993	O75	1.708
O76	1.842	O77	2.081	O78	1.910
O79	1.889	O80	1.828	O81	1.960
O82	1.798	O83	2.166	O84	1.904
O85	1.909	O86	1.885	O87	1.783
O88	1.830	O89	1.860	O90	1.857
O91	2.112	O92	1.867	O93	1.806
O94	1.807	O95	1.750	O96	1.825
O97	2.066	O98	1.988	O99	1.936
O100	1.591	O101	1.703	O102	1.613
O103	2.012	O104	1.466	O105	1.703
O106	1.749	O107	1.919	O108	1.904
O109	1.847	O110	1.890	O111	1.745
O112	1.613	O113	1.750	O114	1.703

O115	1.749	O116	1.847	O117	1.786
O118	1.926	O119	1.898	O120	1.657
O121	1.955	O122	1.957	O123	1.855
O124	1.613	O125	1.964	O126	1.865
O127	1.587	O1W	0.262	O2W	0.284
O3W	0.270				

Table S2. The results of BVS calculations of all O atoms in **2a**.

Atom	BVS	Atom	BVS	Atom	BVS
O1	1.897	O2	1.963	O3	1.959
O4	2.050	O5	1.852	O6	1.935
O7	1.898	O8	1.984	O9	2.011
O10	1.987	O11	1.976	O12	2.181
O13	1.942	O14	2.066	O15	1.933
O16	2.094	O17	1.613	O18	2.181
O19	2.120	O20	1.882	O21	2.420
O22	2.097	O23	2.094	O24	1.749
O25	2.054	O26	2.094	O27	1.875
O28	1.657	O29	2.291	O30	2.105
O31	1.797	O32	2.068	O33	1.962
O34	2.071	O35	2.064	O36	1.703
O37	1.858	O38	2.171	O39	1.924
O40	1.798	O41	1.907	O42	1.910
O43	1.825	O44	2.049	O45	1.997
O46	1.847	O47	2.020	O48	1.749
O49	1.963	O50	1.987	O51	2.066
O52	1.658	O53	1.857	O54	2.132
O55	1.815	O56	1.965	O57	2.131
O58	1.776	O59	1.897	O60	1.832
O61	2.007	O62	1.824	O63	2.097
O64	2.094	O65	2.083	O66	1.955
O67	2.330	O68	1.749	O69	1.944
O70	1.703	O71	2.155	O72	1.965
O73	2.254	O74	1.749	O75	1.858
O76	1.959	O77	1.854	O78	2.010
O79	1.897	O80	2.025	O81	1.657
O82	2.204	O83	1.874	O84	2.293
O85	2.000	O86	1.995	O87	1.934
O88	1.749	O89	1.449	O90	1.963
O91	1.749	O92	1.570	O93	1.978
O94	0.995	O95	2.015	O96	2.097
O97	1.749	O98	1.962	O99	1.788
O100	2.332	O101	1.968	O102	1.847
O103	2.057	O104	1.932	O105	2.165
O106	1.987	O107	1.932	O108	1.897
O109	1.915	O110	1.959	O111	2.196
O112	1.750	O113	2.064	O114	2.066
O115	1.613	O116	1.965	O117	2.131
O118	1.883	O119	1.703	O120	1.905
O121	1.602	O122	2.181	O123	1.847
O124	1.932	O125	1.867	O126	1.898
O127	1.852	O128	1954	O129	1.897

O130	2.108	O131	2.477	O132	2.124
O133	1.703	O134	2.043	O135	2.211
O136	1.984	O137	1.750	O138	1.984
O139	2.052	O140	1.965	O141	1.948
O142	1.986	O143	1.487	O144	2.214
O145	1.937	O146	2.002	O147	1.822
O148	1.978	O149	2.088	O150	2.057
O151	1.934	O152	2.114	O153	1.897
O154	2.103	O155	2.150	O156	1.798
O157	1.750	O158	2.122	O159	2.205
O160	2.011	O161	2.011	O162	1.897
O163	2.078	O164	1.657	O165	2.066
O166	2.021	O167	1.657	O168	1.719
O169	1.954	O170	2.012	O171	2.028
O172	1.098	O173	1.966	O174	1.954
O175	1.981	O176	2.119	O177	2.195
O178	1.984	O179	1.905	O180	2.095
O181	2.058	O182	2.292	O183	2.002
O184	1.914	O185	1.864	O186	1.833
O187	1.749	O188	2.068	O189	1.990
O190	1.949	O191	2.062	O192	1.860
O193	1830	O194	1.898	O195	2.034
O196	1.949	O197	2.163	O198	2.068
O199	1.798	O200	1.843	O201	1.934
O202	1.570	O203	2.075	O204	2.330
O205	1.847	O206	2.052	O1W	0.335
O2W	0.308	O3W	0.326	O4W	0.353
O5W	0.394	O6W	0.373	O7W	0.292
O8W	0.300	O9W	0.415	O10W	0.344
O11W	0.394	O12W	0.309	O14W	0.404
O15W	0.269	O16W	0.394	O17W	0.335
O18W	0.262	O19W	0.326	O20W	0.332
O48W	0.262				

Table S3. Comparison of some POM-based catalysts for the catalytic oxidation of MPS with **2.**

Compounds	Time (min)	Temp(°C)	Conve (%)	Sel (%)	Ref.
$[Ce_2(H_2O)_6(DMEA)W_4O_9(\alpha\text{-}SeW_9O_{33})_3]^{12-}$	60	40	100	100	3
$[Ce_2W_4O_9(H_2O)_7(SeW_9O_{33})_3]_2^{24-}$	60	40	100	100	3
$[Zr_{24}O_{22}(OH)_{10}(H_2O)_2(W_2O_{10}H)_2(GeW_9O_{34})_4(GeW_8O_{31})_2]^{32-}$	60	60	99	84	4
$[Ln_3(H_2O)_{14}\{(Mo_8O_{24})(O_3PCH_2COO)_3\}_2]^{9-}$	60	50	100	99.7	5
$[As_4W_{40}O_{140}\{Ru_2(CH_3COO)\}_2]^{14-}$	60	50	100	100	6
$\{Ti_7O_6(SbW_9O_{33})_4\}_2^{40-}$	60	50	100	100	7
$[\{Re(CO)_3\}_4(Mo_4O_{16})]^{4-}$	60	35	99	100	8
$[Na_5Sb_3(Sb_2Mo_{12}O_{57})]^{12-}$	60	25	100	100	9

$\{[W_2Nd_2(H_2O)_8O_6(OH)_2(\beta\text{-}Se_2W_{14}O_{52})][W_3Nd_2(H_2O)_6O_7(B\text{-}\alpha\text{-}SeW_9O_{33})_2]_2\}^{20-}$	10	35	100	100	This paper

1 G. M. Sheldrick, SHELXL 97, Program for Crystal Structure Refinement; University of Göttingen: Göttingen, Germany, 1997.

2 G. M. Sheldrick, SHELXS 97, Program for Crystal Structure Solution; University of Göttingen: Göttingen, Germany, 1997.

3 H.-L. Li, C. Lian, L.-J. Chen, J.-W. Zhao and G.-Y. Yang, *Inorg. Chem.,* 2019*,* **58,** 8442–8450.

4 L. Huang, S.-S. Wang, J.-W. Zhao, L. Cheng and G.-Y. Yang, *J. Am. Chem. Soc.,* 2014, **136**, 7637–7642.

5 J. W. Wang, Y. J. Niu, M. Zhang, P. T. Ma, C. Zhang, J. Y. Niu and J. P. Wang, *Inorg. Chem.,* 2018, 57, 1796–1805.

6 M. D. Han, Y. J. Niu, R. Wan, Q. F. Xu, J. K. Lu, P. T. Ma, C. Zhang, J. Y. Niu and J. P. Wang, *Chem. Eur. J.,* 2018, **24**, 11059–11066.

7 H.-L. Li, C. Lian, D.-P. Yin, Z.-Y. Jia and G.-Y. Yang, *Cryst. Growth Des.,* 2019, **19**, 376–380.

8 J. K. Lu, X. Y. Ma, V. Singh, Y. J. Zhang, P. T. Ma, C. Zhang, J. Y. Niu and J. P. Wang, *Dalton Trans.,* 2018, **47**, 5279–5285.

9 J. K. Lu, Y. P. Wang, X. Y. Ma, Y. J. Niu, V. Singh, P. T. Ma, C. Zhang, J. Y. Niu and J. P. Wang, *Dalton Trans.*, 2018, **47**, 8070–8077.